Supplementary Materials for

Superhydrophobic turbulent drag reduction as a function of surface grating parameters

Hyungmin Park, Guangyi Sun, and Chang-Jin "CJ" Kim

Mechanical and Aerospace Engineering Department, University of California at Los Angeles, (UCLA), Los Angeles, CA 90095, USA

Figure S1. Schematic figure of a sample consisting of a SHPo surface and a smooth surface each suspended by an identical set of eight flexure beam springs. The sample is fixed to a viewing window with spacers, so that the floating (suspended) surfaces can displace to the flow direction, as illustrated by the cross-sectional view (drawn not to scale).

Figure S2. (a) Geometry of the micrograte structures aligned to the flow direction for SHPo surface. (b) Cross-sectional SEM image of the microgrates (50 μm pitch and 80% *GF*) on an actual SHPo surface used for flow testing.

Figure S3. Cross-sectional schematic of the sample, showing a SHPo surface and a smooth (reference) surface each suspended by an identical spring of flexure beams, all carved out monolithically from silicon by lithography. The frame of the surfaces is glued on spacers on a glass plate, through which the surfaces are directly observed. Water is on top in this figure, not drawn to scale.

Figure S4. (a) Cross-sectional schematic of plug assembly with the sample flush-mounted on the top inside wall of water tunnel. (b) Photographs of the water-tunnel setup and the plug assembly (looking down through the viewing window from above the water tunnel) during the flow test. (c) Photograph of plug assembly viewed from the sample side.

Figure S5. Mean streamwise velocity (in wall units, shown with y^+ drawn in log scale) measured at varying distances from the wall, obtained at the leading edge of the sample. It is confirmed that the flow above the current sample is turbulent. Furthermore, there is no effect of possible adverse pressure gradient, i.e., no apparent wake region.

Figure S6. Mean streamwise velocity (normalized in real units) measured at the leading edge of the sample, compared with those of Blasius solution in laminar flows and $1/7^{th}$ power law in turbulent flows. The result again confirms a TBL flow.

Figure S7. Temporal displacements (i.e., skin-friction drags) of the SHPo (●) and smooth (□) surfaces: (a) *GF* = 30%; (b) 50%; (c) 60%; (d) 70%; (e) 80%; (f) 90%; (g) 95%. Here, the pitch of the microgrates is fixed at 50 μm. The solid lines denote the time-averaged displacements of the floating surfaces.

Figure S8. Temporal displacements (i.e., skin-friction drags) of the SHPo (●) and smooth (□) surfaces: (a) *GF* = 50%; (b) 70%; (c) 90%; d) 95%. Here, the pitch of the microgrates is fixed at 100 μm. The solid lines denote the time-averaged displacements of the floating surfaces.

Supplementary Movie 1. Comparative displacement of a SHPo surface and a smooth surface measured in in a turbulent boundary layer flow ($Re_\tau \sim 250$) – 50× slower. It is clearly seen that the SHPo surface (50 μm pitch and 90% *GF*) is dragged less than a smooth counterpart in a turbulent flow which indicates a skin-friction drag reduction.

Sample for Comparative Measurement of Shear-Forces In this study, each of the time-averaged values (i.e., for all the data points in Fig. 3(a)) is obtained using one sample designed and fabricated for one set of SHPo geometric parameters. A sample consists of two floating surfaces each suspended by an identical spring of eight flexure beams, as schematically described in Fig. S1. Due to the high *t*/*w* ratio of the flexure beams and the long rigid beams bridging the flexure beams, the floating surface is allowed to move along the longitudinal (parallel to the flow) direction but highly restricted against transverse, vertical, and rotational motions. Ruler marks were lithographically patterned on the other side of the sample (away from the flow), so that the displacements can be measured from outside the water tunnel through a transparent viewing window with a reading resolution better than 3 μm. In comparison, previous attempts to measure the skin friction with floating elements used complex electrical transductions to achieve standalone micro-sensors (Naughton & Sheplak 2002). The direct and comparative measurement in this study avoids the complexities of implementing sensors and the errors associated with them. The design, modeling, and calibration of the sensing device will be reported elsewhere (Sun *et al*. 2013).

Analysis on the Secondary Effect of Induced Flow in Spanwise Direction over the Sample Because the SHPo surface is surrounded by smooth surfaces, the pressure gradient caused by the difference in the wall-shear stresses might induce a spanwise flow to the SHPo surface. Let us first perform a rough order-of-magnitude analysis for the time scales corresponding to the main (streamwise) and induced (spanwise) flows. The time scale for the main flow is defined as $\tau_{streamwise} = L/u_\infty$, where L is the streamwise length of the SHPo surface and u_∞ is the free-stream velocity. On the other hand, the time scale for the induced flow, if any, is defined as $\tau_{spanwise} = l/v_{ind}$, where l is the spanwise distance between the smooth and the surrounding smooth surfaces and v_{ind} is the induced velocity in spanwise direction. From the Bernoulli relationship, we can roughly estimate the v_{ind} as $v_{ind} \sim \sqrt{\Delta p} \sim \sqrt{\Delta u^2} \sim \sqrt{\Delta u_\tau^2} = \sqrt{\Delta \tau_w / \rho}$ (here p is the pressure and Δ denotes the difference between smooth and SHPo surfaces), leading to $\tau_{streamwise}/\tau_{spanwise} \sim (L/l)(1/u_\infty)\sqrt{\Delta \tau_w/\rho}$. Since this time-scale ratio is calculated to be less than 2% for all the results in the present study, we conclude that the effect of the induced flow on the free stream is very small. Let us next perform an order-of-magnitude analysis for the overestimation of the SHPo drag due to the increased streamwise flow on the slip surface by the spanwise inflow from the surrounding no-slip surfaces. The increased drag by the added flow can be approximated as $\Delta D/D \sim \Delta u^2/u^2 \sim \Delta \tau_w/\rho u^2$. Considering the drag results obtained in the present study, the overestimation of the SHPo drag due to the secondary effect of the induced flows is estimated to be less than 0.2% for all the cases. Therefore, we conclude that the effect of induced flows on the measurement of the SHPo drag using the current comparative sample is negligible.

SHPo Surfaces Despite the numerous SHPo surfaces in the literature, only a few can provide a surface slip large enough to consider any drag reduction. The SHPo surfaces in this study are of

micro-scale grates (microgrates) aligned to the streamwise (parallel to the flow) direction (Lee *et al*. 2008), as shown in Fig. S2. The 50 μm or 100 μm pitch was large enough to induce a significant slip but small enough to keep the air-water interface intact for hours (Lee *et al*. 2008), and the alignment to the streamwise direction produced a larger slip for a given micrograte surface (Lauga & Stone 2003). The slip in the spanwise (transverse to the flow) direction was smaller and found inducing a smaller drag reduction in laminar flows (Choi *et al*. 2006; Davies *et al*. 2006; Woolford *et al*. 2009a). However, the role of the spanwise slip is more complicated in turbulent flows. Testing in turbulent channel flows, Woolford *et al*. (2009b) found that the friction factor on transverse microgrates is not only greater than what occurs on longitudinal microgrates, but also greater than what occurs on smooth surfaces. The spanwise slip was numerically shown to strengthen near-wall streamwise vortices and consequently increase the skin-friction drag in turbulent flows (Min & Kim 2004; Busse & Sandham 2012). We chose longitudinal grates, expecting they would outperform other surfaces such as posts and irregular structures in terms of turbulent drag reduction.

Fabrication of Sample The drag-reduction measurement sample was monolithically fabricated from a silicon wafer. Starting with a double-side polished 200 μm-thick silicon wafer, flexure beams were defined by deep reactive ion etching (DRIE) on one side using a photoresist as the etching mask. This etching step also patterned the built-in ruler marks. After dicing the wafer into several 27 mm × 27 mm chips – each to be a sample, the chip is flipped over and glued on a handle wafer. Another DRIE was performed to etch through the chip from the other side. This step not only defined the two floating surfaces but also created the microgrates on top of the SHPo surface. After dissolving the glue to free the chip from the handle wafer, the chip was coated with Teflon® and baked, which made all the exposed surfaces hydrophobic and the microgrates surface SHPo. We used a 0.2% Teflon by diluting Dufont™ Teflon® AF in a perfluorinated solvent (FC-40). At last, the sample chip was epoxy-glued on a transparent acrylic window with a 300 μm gap formed by glass spacers. Details on micromachining and characterization of the samples will be reported elsewhere.

Water Tunnel A series of flow tests have been performed in a water tunnel (flowLab™, MSE Inc., USA), using an industrial tap water. The flowing water was likely saturated with the ambient air, prolonging the SHPo state of the immersed sample to hours without wetting the microgrates. Turbulent boundary layers (TBLs) flew along the inside walls of its test section. The flowLab™ is a closed-type, small-size water tunnel whose test section is 610 mm × 50 mm × 50 mm in the streamwise, vertical, and spanwise directions, respectively. The sample was located upside down at the upper wall of the test section, 450 mm downstream of the tunnel inlet, as illustrated in Fig. S4(a). At the tested flow condition, the Reynolds number above the sample was $Re_x \sim 2 \times 10^5$, corresponding to the frictional Reynolds number of $Re_\tau \sim 250$, based on the friction velocity (u_τ) and local boundary layer thickness at the leading edge of the sample. The

friction velocity was calculated by fitting the measured boundary-layer profile onto the log-law equation. The background turbulence level in the free stream was measured to be about 5% at the considered speed.

Confirmation of the TBL flow To confirm that the flow over the sample during the flow tests is of TBL, the boundary-layer profile was measured at the leading edge of the sample using laser Doppler velocimetry (LDV). The measurement was done by a miniLDV-G5-100 probe (MSE Inc.) with a measurement standoff distance of 100 mm. The probe was tilted upward (approximately 15 degrees) in order to reach the designated measurement point. The experiment was carried out without use of the frequency shifting of the probe. The miniLDV probe was attached to a vertical traverse that is PC-controlled and run by the miniLDV processing software. The velocity profile was obtained from 12 mm away from the top surface of the sample to as close to the wall as possible. The measurement location increments were in 50 μm steps. The processing software collected 2000 Doppler samples at each position and provided the data for the mean velocity (Figs. S5 and S6). As shown in Fig. S5, the boundary-layer profile satisfies the "log law", confirming the flow is fully turbulent. The higher turbulence intensity (5%) than a typical value (below 0.1%) in the water channel allowed a fully turbulent flow at $Re_x = 2 \times 10^5$, which is somewhat lower than the typical textbook value ($Re_x = 3 \times 10^5$), without tripping the flow at the inlet. Furthermore, no adverse pressure gradient is found, as expected from the negligibly small wake region in the mean velocity profile (Krogstad & Skåre 1995), confirming the flow as a TBL flow. As an additional examination for turbulence, Fig. S6 presents the flow velocity data in normalized real units to compare with the Blasius solution of laminar flows and the $1/7^{th}$ power law of turbulent flows. The result again confirms a TBL flow.

Plug Assembly To flush-mount the sample to the inside wall of the test section and enable optical measurement of surface displacements from outside, we developed a plug assembly machined from stainless steel and acrylic. The plug assembly is viewed from the sample side in Fig. S4(c) and from outside the water tunnel during the flow tests in Fig. S4(b). The cross-sectional view of the plug in Fig. S4(a) illustrates how the assembly is installed in the water tunnel, how the sample is flush with the inside wall, and how the displacement of the floating surfaces can be measured directly. For the sensing mechanism to work as designed, it is important to prevent the water from seeping into the gap between the sample and viewing window. To achieve this, a hydrophobic coating was applied not only to the top surfaces but to all surfaces of the sample, including the sidewalls of flexure beams and backside of the sample where rulers are patterned. Furthermore, a small (200 μm in diameter) breathing holes was drilled through the viewing window behind each floating surface to minimize the pressure build up and moisture condensation in the gap between the sample and the viewing window. During the flow tests, the gap was visually confirmed to be free of water filling.

Calculation of Drag Reduction (DR) Based on the relationship between the skin-friction drag (F_s) and displacement (d) of the floating surface, the normalized drag on SHPo surface was calculated which is related to the DR as below;

$$\mathrm{DR} = 1 - \frac{\bar{d}_{\mathrm{SHPo}}}{\bar{d}_{\mathrm{smooth}}} = 1 - \text{normalized drag} \qquad \text{(S1)}$$

where the upper bar denotes the time-averaged value. Each of the time-averaged data (Fig. 3a) was obtained from the temporal variation of skin-friction drags on each sample (Figs. S7 and S8).

References

Davies, J., Maynes, D., Webb, B. W. & Woolford, B. 2006 Laminar flow in a microchannel with superhydrophobic walls exhibiting transverse ribs. *Phys. Fluids* **18**, 087110.

Krogstad, P.-Å. & Skåre, P. E. 1995 Influence of a strong adverse pressure gradient on the turbulent structure in a boundary layer. *Phys. Fluids* **7**, 2014-2024.

Park, H., Sun, G. & Kim, C.-J. 2013 Turbulent drag reduction on superhydrophobic surfaces confirmed by built-in shear sensing. *Proc. IEEE Int. Conf. MEMS*, Taipei, Taiwan, Jan. 2013, pp. 1183-1186.

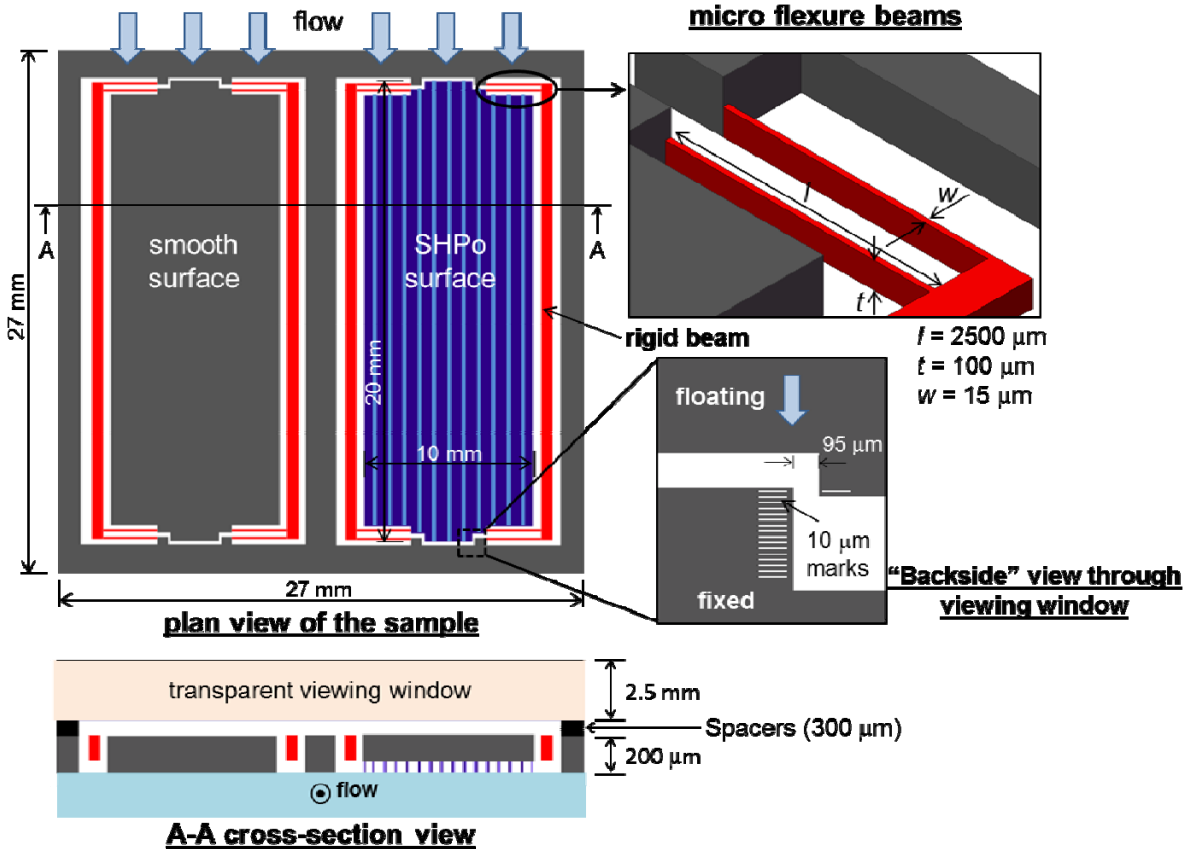

Figure S1. Schematic figure of a sample consisting of a SHPo surface and a smooth surface each suspended by an identical set of eight flexure beam springs. The sample is fixed to a viewing window with spacers, so that the floating (suspended) surfaces can displace along the flow direction, as illustrated by the cross-sectional view (drawn not to scale).

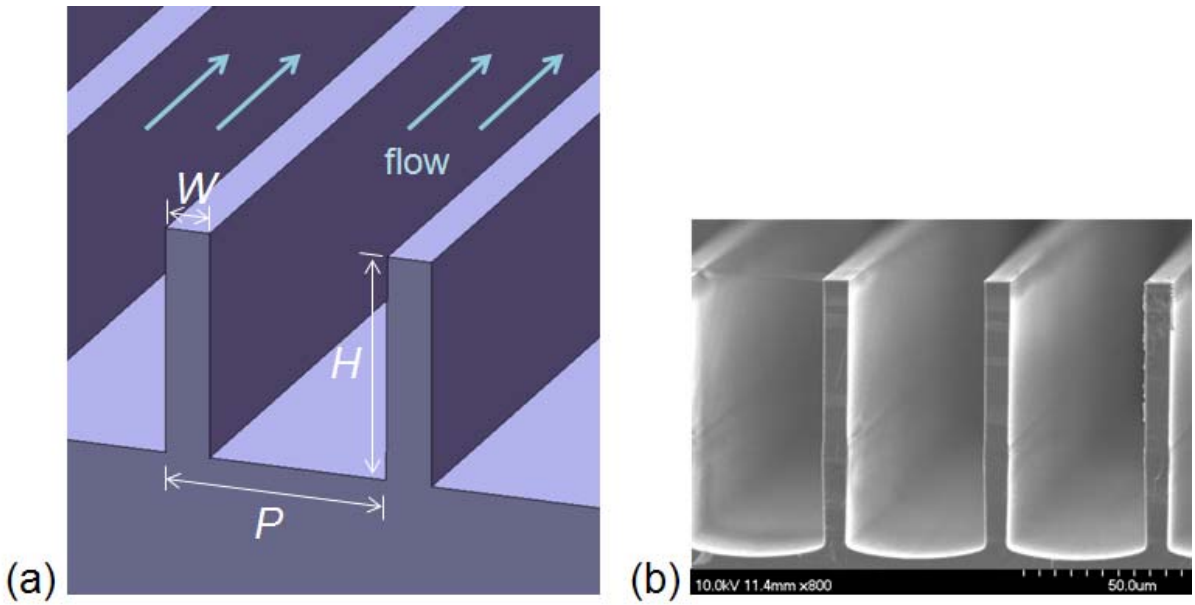

Figure S2. (a) Geometry of the micrograte structures aligned to the flow direction for SHPo surface. (b) Cross-sectional SEM image of the microgrates (50 μm pitch and 80% *GF*) on an actual SHPo surface used for flow testing.

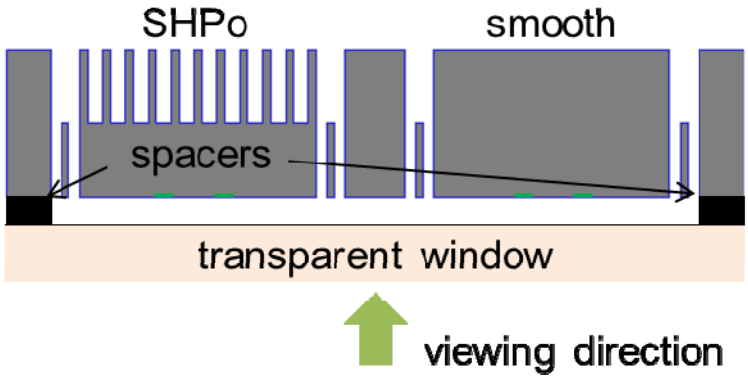

Figure S3. Cross-sectional schematic of the sample, showing a SHPo surface and a smooth (reference) surface each suspended by an identical spring of flexure beams, all carved out monolithically from silicon by lithography. The frame of the surfaces is glued on spacers on a glass plate, through which the surfaces are directly observed. Water is on top in this figure, not drawn to scale.

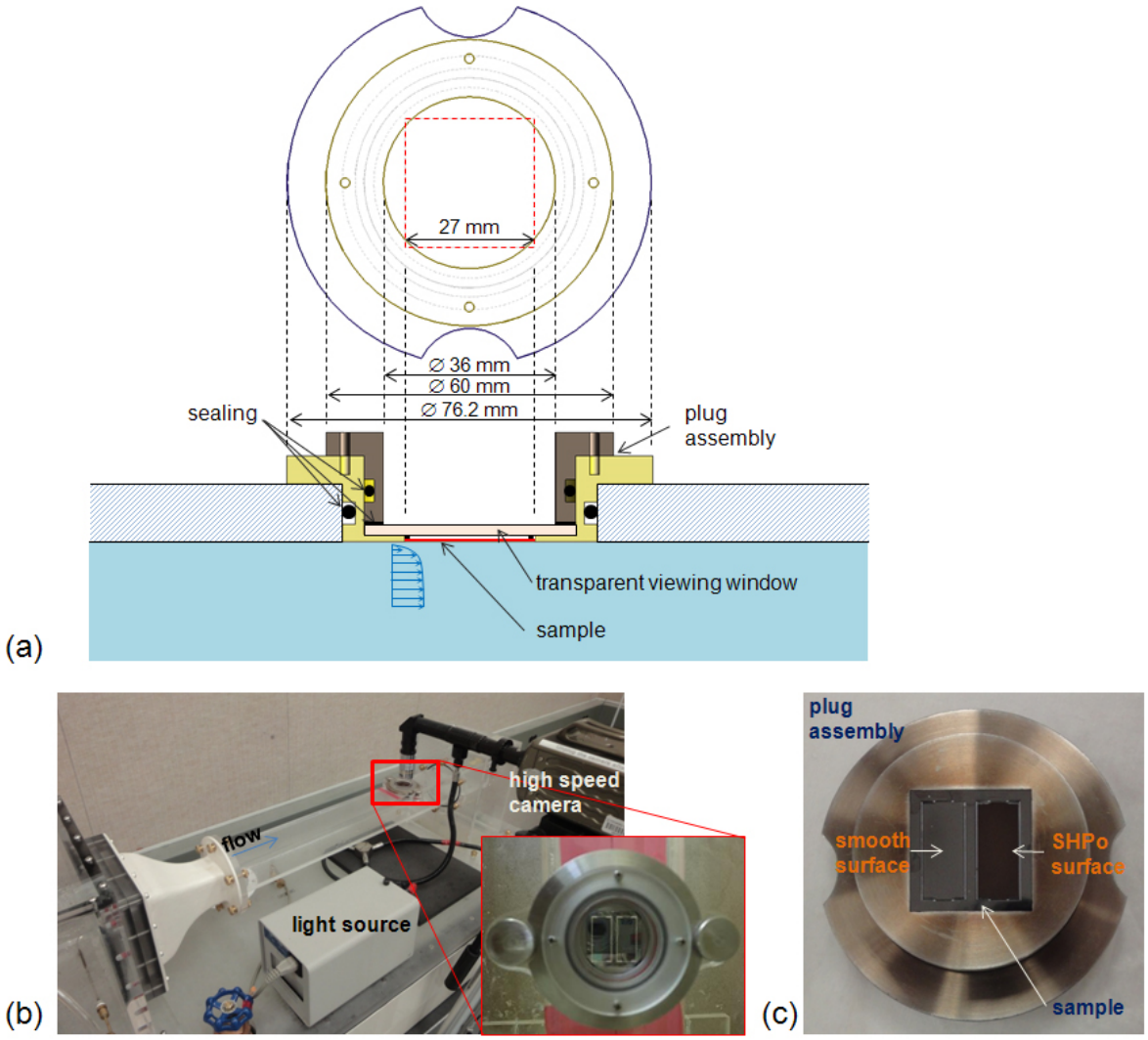

Figure S4. (a) Cross-sectional schematic of plug assembly with the sample flush-mounted on the top inside wall of water tunnel. (b) Photographs of the water-tunnel setup and the plug assembly (looking down through the viewing window from above the water tunnel) during the flow test. (c) Photograph of plug assembly viewed from the sample side.

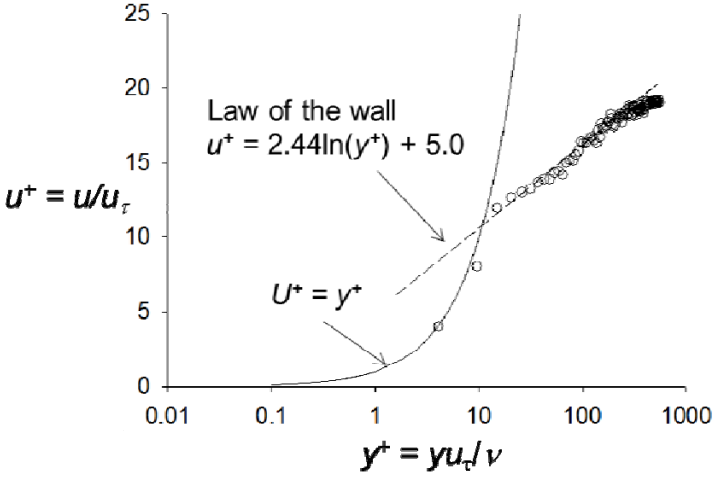

Figure S5. Mean streamwise velocity (in wall units, shown with y^+ drawn in log scale) measured at varying distances from the wall, obtained at the leading edge of the sample. It is confirmed that the flow above the current sample is turbulent. Furthermore, there is no effect of possible adverse pressure gradient, i.e., no apparent wake region.

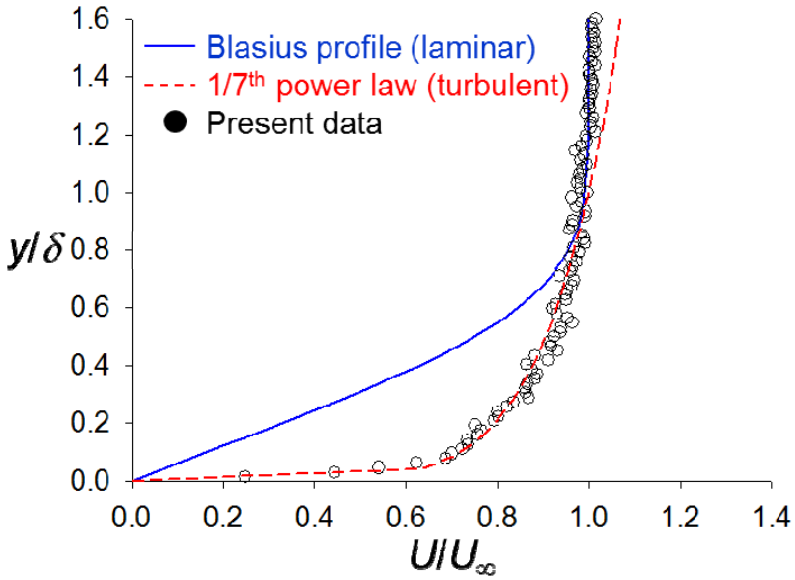

Figure S6. Mean streamwise velocity (normalized in real units) measured at the leading edge of the sample, compared with those of Blasius solution in laminar flows and 1/7th power law in turbulent flows. The result again confirms a TBL flow.

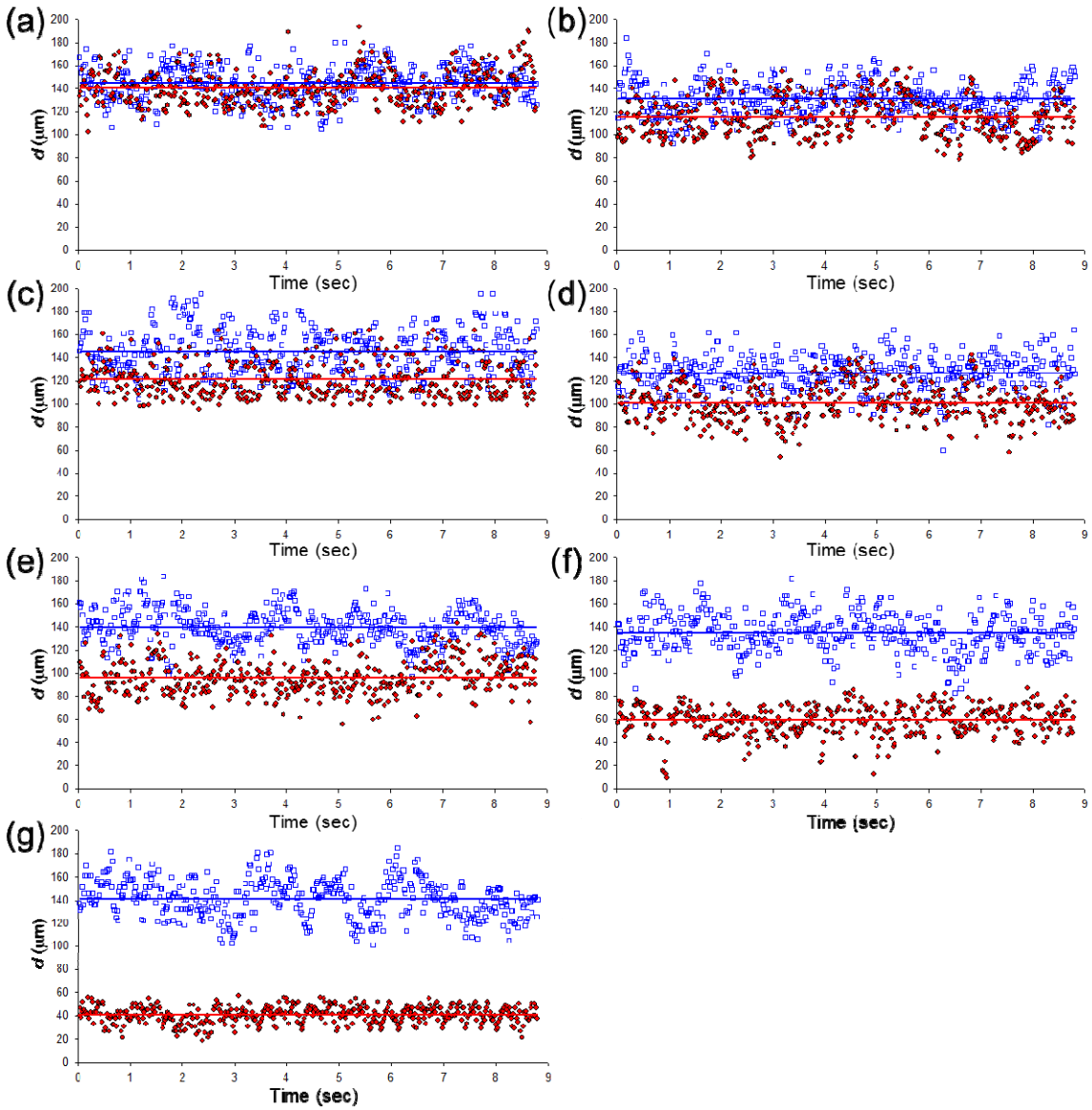

Figure S7. Temporal displacements (i.e., skin-friction drags) of the SHPo (●) and smooth (□) surfaces: (a) *GF* = 30%; (b) 50%; (c) 60%; (d) 70%; (e) 80%; (f) 90%; (g) 95%. Here, the pitch of the micrograte is fixed at 50 μm. The solid lines denote the time-averaged displacements of the floating surfaces.

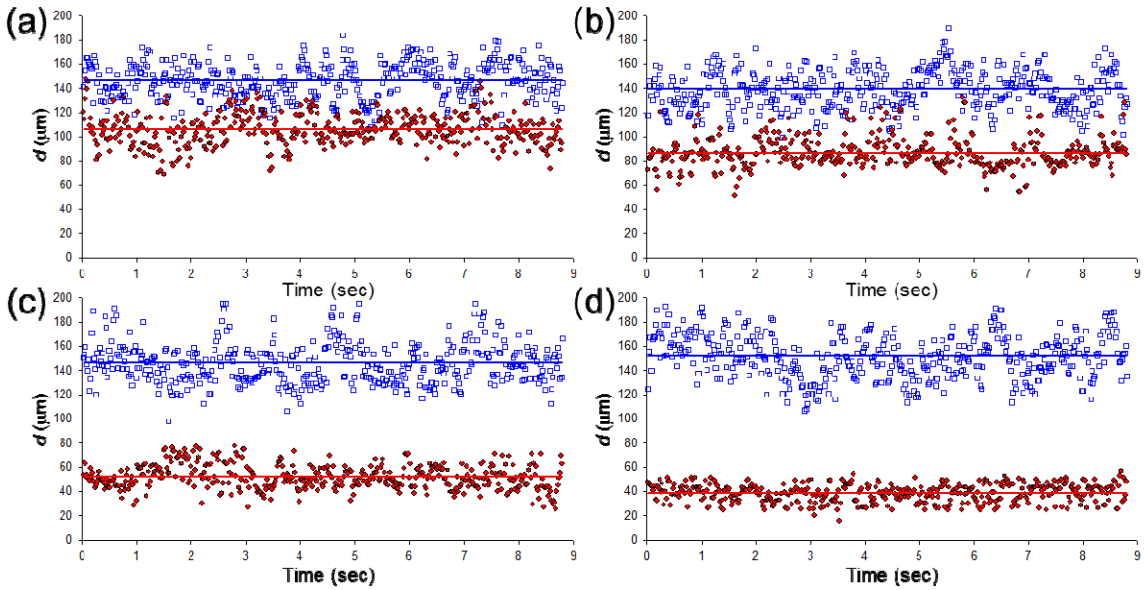

Figure S8. Temporal displacements (i.e., skin-friction drags) of the SHPo (●) and smooth (□) surfaces: (a) *GF* = 50%; (b) 70%; (c) 90%; (d) 95%. Here, the pitch of the microgrates is fixed at 100 μm. The solid lines denote the time-averaged displacements of the floating surfaces.